A bio-inspired sand-rolling robot: effect of body shape on sand rolling performance

Xingjue Liao[1], Wenhao Liu[1], Hao Wu[1] and Feifei Qian[*,1]

Abstract*—The capability of effectively moving on complex terrains such as sand and gravel can empower our robots to robustly operate in outdoor environments, and assist with critical tasks such as environment monitoring, search-and-rescue, and supply delivery. Inspired by the Mount Lyell salamander's ability to curl its body into a loop and effectively roll across sand and gravel, in this study we develop a sand-rolling robot and investigate how its locomotion performance is governed by the shape of its body. We experimentally tested three different body shapes: Hexagon, Quadrilateral, and Triangle. We found that Hexagon and Triangle can achieve a faster rolling speed on sand, but also exhibited more frequent failures of getting stuck in sand. Analysis of the interaction between robot and sand revealed the failure mechanism: the deformation of the sand produced a local "sand incline" underneath robot contact segments, increasing the effective region of supporting polygon (ERSP) and preventing the robot from shifting its center of mass (CoM) outside the ERSP to produce sustainable rolling. Based on this mechanism, a highly-simplified model successfully captured the critical body pitch for each rolling shape to produce sustained rolling on sand, and informed design adaptations that mitigated the locomotion failures and improved robot speed by more than 200%. Our results provide insights into how locomotors can utilize different morphological features to achieve robust rolling motion across deformable substrates.

***Index Terms*—Biologically-Inspired Robots; Locomotion on Deformable Terrains; Contact Modeling**

I. INTRODUCTION

Deformable substrates such as sand, dirt, and soil exist widely in both Earth and extraterrestrial environments (Fig. 1a, b). The ability for robots to successfully and robustly move across deformable substrates can empower our robots for a variety of critical missions in agriculture, transportation, post-disaster search-and-rescue, and environment monitoring. However, moving on deformable substrates can be extremely challenging, as the substrates can exhibit both solid-like and fluid-like behaviors [1], leading to sinkage, slippage, and other complex locomotor-terrain interactions [2], [3]. Misapplied locomotion strategies can lead to catastrophic failures [4].

Many biological locomotors (Fig. 1c, d) exhibit high locomotion performance on deformable substrates [5]–[10]. Their morphology and strategies have inspired bio-inspired designs and controls for robot locomotion on complex terrains [7]–[9], [11]–[16]. Among the high-performance animals on sand, the *Batrachoseps attenuaturs* Salamander and *Hydromantes platycephalus* (Mount Lyell Salamander) [17], [18] (Fig. 1d) use an distinct strategy: by curling up their body into a circle, they are able to agily and stably roll down soft sand dunes and rugged rocky hills.

Fig. 1. Deformable substrates in Earth and extraterrestrial environments, and animals that exhibit high locomotion performance in these environments. (a) Loose regolith on Mars. Image credit NASA/JPL-Caltech/ASU/MSSS. (b) Sand dunes in California desert. Image credit Wikimedia Commons. (c) Sceloporus, a generalist lizard with high locomotion performance on sand [8]. Image credit Wikimedia Commons. (d) *Batrachoseps attenuaturs*, a salamander that can agily roll down sand dunes and rugged hills. Image credit Wikimedia Commons.

Intrigued by the salamander's interesting locomotion mode and high performance, we seek to understand the principles governing self-propelled rolling performance on sand. Many previous studies have proposed designs for rolling robots. One common design is to control the joint angles between closed-chain segments to achieve rolling [19]. Another study proposed a mechanism that uses a center-arranged actuator to drive the connection between inner crank links and outer chain. Rather interestingly, the JSEL [20] robot achieved self-propelled rolling by locally deforming its surface cells through jamming and unjamming. In most of these studies, the rolling robot was developed for and tested on relatively simple terrains that are mostly rigid and flat. How deformable substrates would influence rolling robot performance remains an under-explored question.

To address this gap, in this paper we compared the locomotion performance of a rolling robot on rigid and deformable substrates (Sec. II), and identified unique challenges for sand-rolling. To understand how sand-rolling performance was affected by robot morphology, we investigated three different robot shape kinematics. Based on observed robot-substrate interactions and resulting performance, we proposed a sim-

[1]Xingjue Liao, Wenhao Liu, Hao Wu and Feifei Qian are with Department of Electrical and Computer Engineering, University of Southern California, Los Angeles, CA, USA. feifeiqi@usc.edu (*corresponding author: Feifei Qian*)

plified model that revealed the failure mechanism of sand-rolling (Sec. III), and demonstrated model-informed design adaptations that resulted in significantly improved sand-rolling performance (Sec. IV).

II. Materials and Methods

A. Robot

To investigate how body morphology affects sand-rolling performance, we developed a bio-inspired robot as a robophysical [21] model to perform controlled locomotion experiments. Modelled after the tumbling lizards which can bend their bodies into a closed loop, the sand-rolling robot was designed with 6 joints to form a closed chain (Fig. 2a, b). Each joint was actuated by a servo motor (Dynamixel XL-320) which was controlled using a microcontroller (Arduino Uno). The length between each pair of adjacent joint axes was 5.6 cm. In this study, we were primarily interested in studying the rolling performance along the fore-aft direction, and thus the width of each segment was chosen to be sufficient wide (W = 7.2 cm) to prevent rotation along x-direction. Three robot body shapes were tested to study how body shape affects sand-rolling performance: a "Triangle" shape (Fig. 3a), a "Quadrilateral" shape (Fig. 3b), and a "Hexagon" shape (Fig. 3c). The kinematics of the robot for each shape are shown in Fig. 3i-iv. A total of 36 trials were performed, 12 for each shape. Among those 12 trials, 6 were performed on rigid ground and another 6 on deformable substrates (see Sec. II-B). For all trials in this study, the robot stride period was set to be 3 seconds.

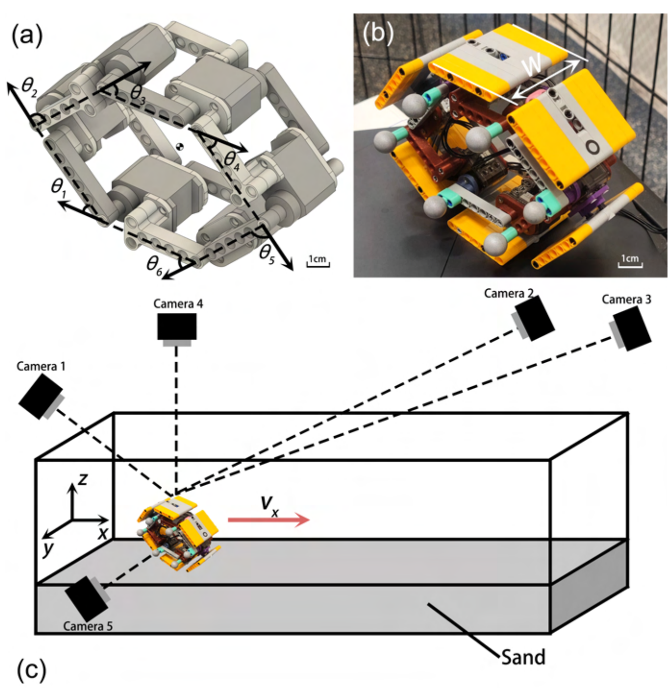

Fig. 2. Sand-rolling robot, and experimental setup to study its sand-rolling performance. (a) Simplified 3D model of the rolling robot. (b) Snapshot of the rolling robot. 6 reflective markers were attached at the six joints of the robot for tracking. (c) Diagram of the granular trackway for testing robot locomotion on sand. Camera 1-3 were used for record tracking data, whereas camera 4-5 were used to record top view and side view experimental footage.

B. Experiment Setup

Robot locomotion experiments were performed in a 125 cm long × 65 cm wide × 17 cm deep trackway (Fig. 2c). Plastic "sand particles" with 6 mm particle diameter were used as a model granular substrate in this study. The 6 mm plastic particles have been proven to be a promising model substrate for studying the interaction between robots and granular materials [5], [11], as they behave qualitatively similar in terms of rheology and forces [22] with natural sand/soil with more angularity and size polydispersity, while the simpler geometry facilitates the control of the substrate to achieve uniform packing state [23]. To ensure a consistent initial condition for each locomotion test, prior to each trial we manually loosen the particles across the trackway prior to each trial, then flatten the surface to eliminate surface height variations.

To characterize the robot speed during sand rolling, three motion capture cameras (Optitrack, Prime 13W) were installed around the trackway to record the position of each joint in the world frame (x_i - fore-aft; y_i - lateral; z_i - vertical, where i is the joint index) at 120 frames per second (FPS). Robot center-of-mass (CoM) position in the world frame (x_c - fore-aft; y_c - lateral; z_c - vertical) was then computed as the geometric center of all joints. In addition, two video camera (Optitrack, Prime Color) were used to record experiment footage from both top view and side view at 120 FPS.

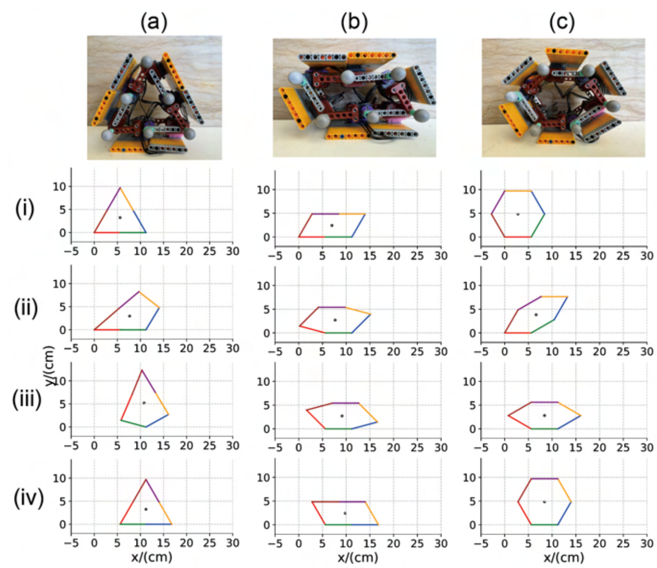

Fig. 3. The kinematics of the three body shapes: (a) Triangle, (b) Quadrilateral, (c) Hexagon.

III. Results and Discussion

A. Effect of robot shape on rolling performance

Tracked robot speed on rigid ground showed that among the 3 shapes Hexagon exhibited the fastest forward speed (v_x = 12.3 ± 3.7 cm/s), followed by Triangle (v_x = 9.4 ± 2.2 cm/s), and Quadrilateral being the slowest (v_x = 5.6 ± 1.6 cm/s). Here v_x is the magnitude of rolling speed along x

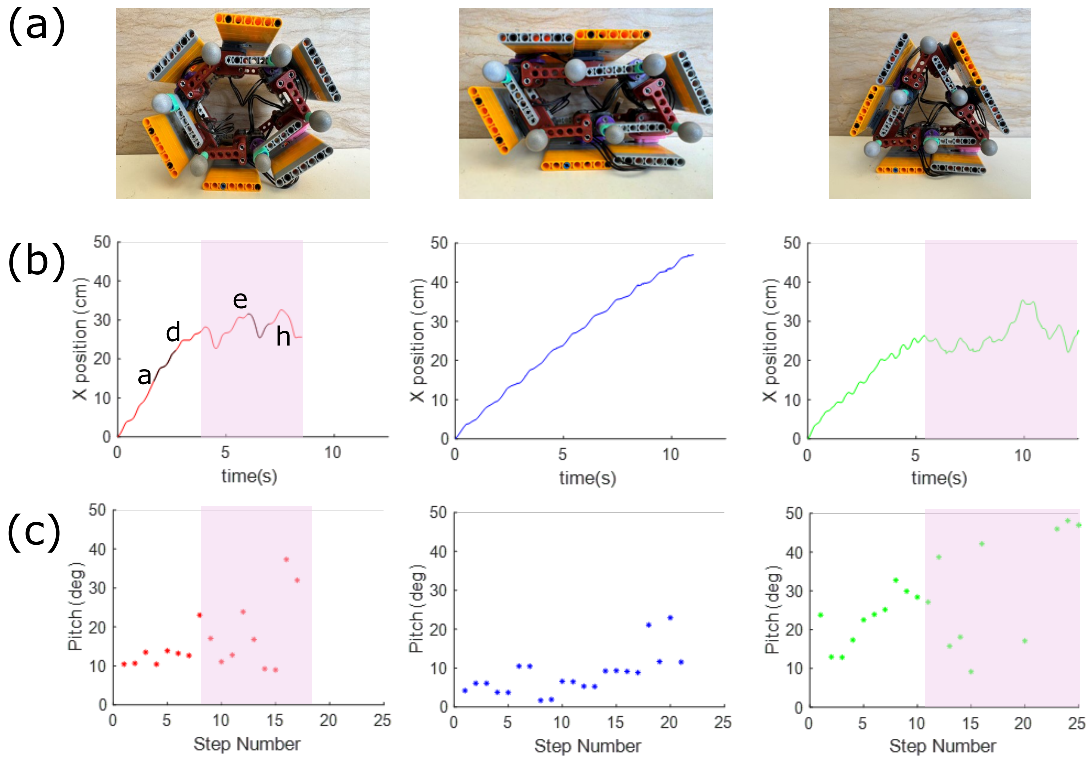

Fig. 4. Representative trials of the robot locomotion on sand with three different shapes: **Left**: Hexagon; **Middle**: Quadrilateral; **Right**: Triangle. **(a)** images of each shape. **(b)** Experimentally-measured robot x-direction position vs. time. The highlighted segment labeled with letter a to d corresponds to experimental images a-d in Fig.5. The highlighted segment labeled with letter e to h corresponds to experimental images e-h in Fig.5. **(c)** Instantaneous body pitch angle measured from each step on sand. In (b) and (c), pink shaded regions represent the "failure region", where the robot oscillated in place and not able to effectively move forward.

direction (Fig. 2c), averaged through each step. The recorded robot speeds on rigid ground are shown in Table. I.

Interestingly, the robot's rolling performance on sand was significantly different from its performance on rigid ground. Specifically, the best-performing shape on rigid, Hexagon, failed to move past 20 cm in 83% of the trials, as shown in Table. I, with an averaged speed[1] of v_x = 1.3 ± 1.0 cm/s. Similar to Hexagon, the Triangle shape exhibited a relatively high failure rate (67%) on sand, with an averaged speed of v_x = 1.5 ± 1.3 cm/s (Table. I). On the other hand, the "worst-performing" shape on rigid ground, Quadrilateral, was able to successfully travel across the entire length of the testing field without any failure, with an averaged speed of v_x = 3.4 ± 0.6 cm/s (Table. I).

A close analysis of the robot fore-aft position vs. time showed that the Hexagon and Triangle could effectively move forward initially in all trials. However, after a few steps they would quickly enter the failure mode (Fig. 5b, pink shaded region), where the robot oscillated in place and could not roll forward. It was also noticed that when the robot could reliably move forward, its body pitch angle was generally small, but as it entered the oscillating failure mode, its body pitch angle from the previous step became significantly larger (Fig. 5c).

[1]Here the averaged robot speed was computed from steps prior to the stopping criteria: (1) completed the entire test range; 2. collided with the side wall of the trackway; 3. fell sideways or exhibited significant turning such that cannot be reliably tracked by the MoCap system; 4. stuck in place for 2 consecutive stride cycles.

TABLE I
PERFORMANCE COMPARISON OF DIFFERENT SHAPES ON RIGID GROUND AND SAND. HERE THE FAILURE RATE WAS COMPUTED AS THE PERCENTAGE OF TRIALS THAT FAILED TO TRAVERSE MORE THAN 20 CM.

Shape	**Averaged speed on rigid ground (cm/s)**	**Failure rate on rigid ground (%)**	**Averaged speed on sand (cm/s)**	**Failure rate on sand (%)**	**Traversed distance on sand before failure (cm)**
Hexagon	12.3±3.7	0	1.3±1.0	83.3	9.5±9.2
Quadrilateral	5.6±1.6	0	3.4±0.6	0	N/A
Triangle	9.4±2.2	0	1.5±1.3	66.6	15.6±14.0

B. Hypothesized failure mechanism for sand-rolling

Intrigued by the high failure rate of the robots on sand for the Hexagon and Triangle shapes, we examined the interactions between the robot and the deformable substrate, to investigate possible failure mechanisms. Fig. 5 shows a representative trial of the Hexagon rolling robot initialling successfully rolling on sand (Fig. 5 a-d), but eventually exhibited a failure mode where the robot oscillated in place (Fig. 5 e-h).

An interesting phenomena observed from the Hexagon shape experiments was that during the failure steps on sand, the robot body was supported by two sand-contacting segments (Fig. 5e-h, green solid lines) that oscillated towards opposite directions, producing a "clam-like" motion and causing the robot to dig into the sand. This was distinct from robot's movement pattern found on rigid surface and in successful traversal steps on sand, where the robot body was mostly supported by a single segment laying relatively flat on the substrate (Fig. 5a-d, green solid lines).

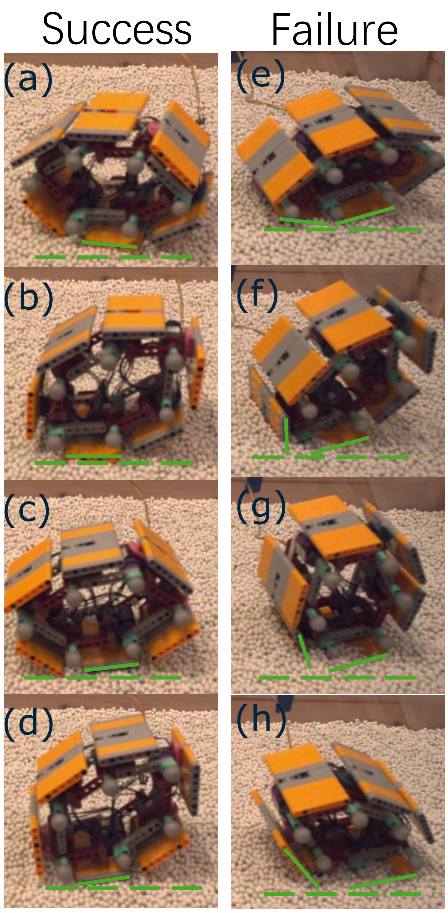

Fig. 5. Image sequence from experimental footage showing a representative trial of Hexagon. **Left**: (a) to (d) illustrate 2 successful steps (corresponding to Fig. 4b highlighted tracking data segment labeled a-d) where the robot continuously rolled forward. Right: (e) to (h) illustrate 2 failing steps (corresponding to Fig. 4b highlighted tracking data segment labeled e-h) where the robot oscillated back and forth in place.

As a result, the body pitch (defined as the angle measured from horizontal plane to the supporting segment) was significantly higher during the failing steps (Fig. 5a-d) as compared to the successful ones (Fig. 5e-h). For robots with the Hexagonal shape, tracked robot body pitch, β, measured from the horizontal sand surface to the robot's lowest body segment at supporting segment-switching moments, remained around 10.0° ± 4.1° for successful steps (*i.e.,* with a stride length greater than 2 cm), but increased significantly to 38.2° ± 18.9 ° for failing steps (*i.e.,* with a stride length below 2cm) (Fig. 5c).

C. Model-predicted critical pitch angle for producing sustainable rolling on sand

Based on the observed high body pitch during failure mode, in this section we propose a simple geometric model to reason about the necessary condition for sustainable rolling, and explain how body pitch influences robot's rolling performance.

In this highly-simplified model, the robot mass was assumed to primarily concentrated at the geometric center (Fig. 6a, b, red circle). To produce sustainable rolling, a necessary condition is that the vertical projection of the robot CoM on the horizontal plane needs to be shifted outside the boundary of the supporting segment (Fig. 6a, b, segment highlighted in green) [24]–[26]. This condition allows the "supporting segment switching", *i.e.,* the touchdown of a new supporting segment, and the lift-off of the previous supporting segment.

On rigid flat ground, the supporting segment was always horizontal to the ground, resulting in a $0°$ body pitch. As a result, all three shape kinematics was able to effectively shift the robot CoM outside the supporting region, achieving supporting segment switching and producing sustained rolling.

On sand, however, the supporting segment was often not horizontal. Granular substrates like sand are yield-stress [27] materials, which behave solid-like if the external stress remains below the yield stress, and flow like fluid when the external stress exceeds the yield stress. As such, during robot rolling, the part of the supporting segment that first reached the sand would begin to deform the substrate, while its penetration depth increased. This created an increased pitch, as if the robot was moving on a slope (Fig. 6b), and increases the effective region of supporting polygon (ERSP). This induced a challenge: a large body pitch created a high virtual slope, making it more difficult for the robot to shift its CoM outside the supporting region and achieve sustained rolling.

We can use the model to predict the maximum pitch angle for each robot shape that can achieve the supporting segment switching. To do so, the robot was fixed on a virtual "ramp" with slope angle β (Fig. 6b), supported by a single segment with full contact with the ramp surface. For each shape, given the robot's kinematics, the model computed the projection of the robot CoM on the ramp surface, and determined the largest ramp angle, β_m, where the CoM projection can be moved outside the ERSP, $[x_l, x_u]$ (Fig. 6b). Here x_l and x_u represent the range of supporting segment on the ramp surface. This largest ramp angle is the maximal pitch angle for each robot shape to produce sustainable rolling on deformable sand. At the supporting segment switching moment, upon the lift-off of the current supporting segment, if the robot instantaneous pitch is larger than β_m, the robot would fail to achieve the supporting segment switching, fell backward, and started to oscillate in place as shown in Fig. 5e-h. We refer to β_m as the critical pitch angle for each shape.

D. Experimentally-measured body pitch for each shape agreed well with model prediction

The model-predicted critical pitch angle for producing sustainable rolling was $\beta_m(hex) = 13.6°$ for the Hexagon, $\beta_m(tri) = 33.4°$ for the Triangle, and $\beta_m(quad) = 39.5°$

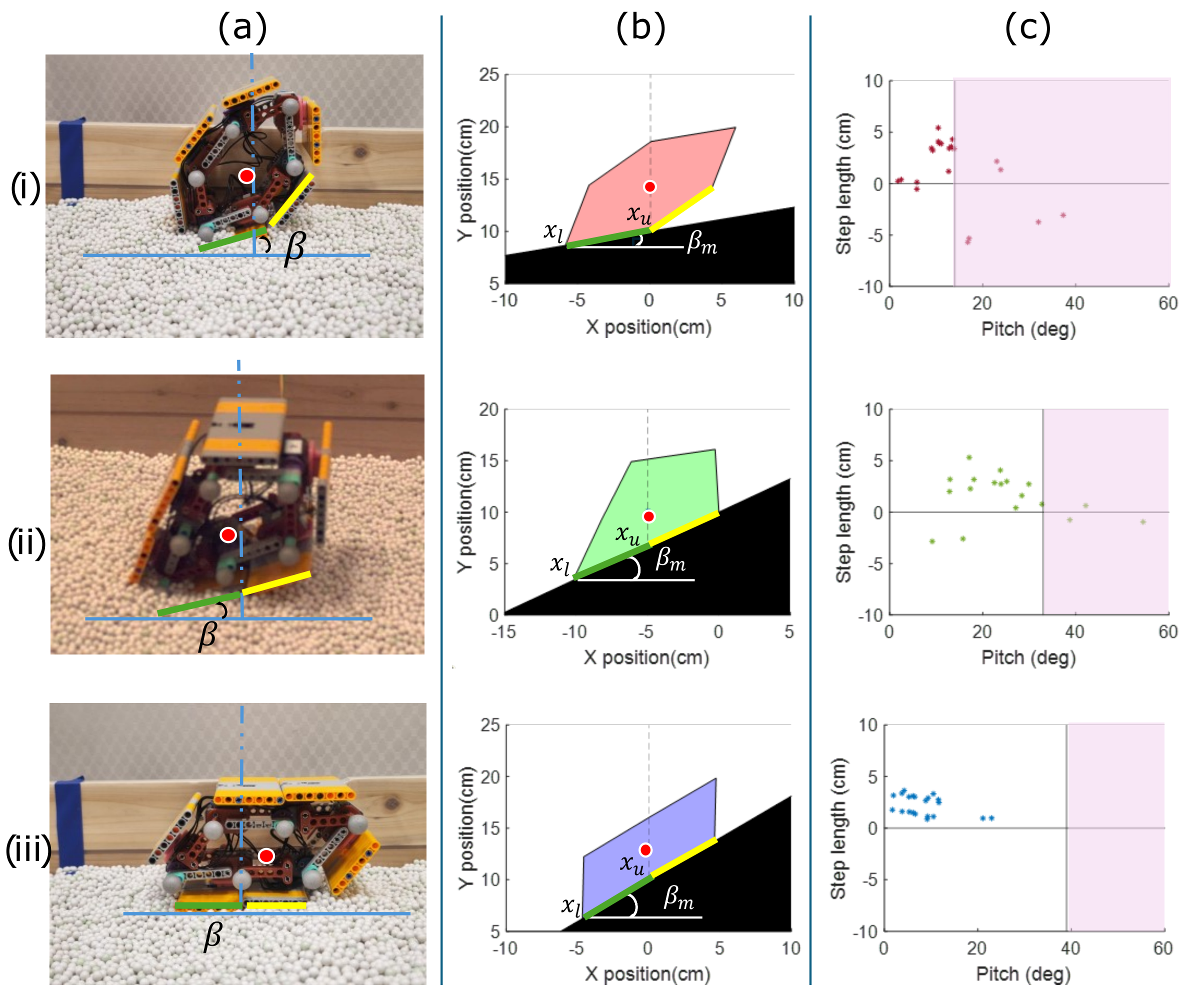

Fig. 6. Proposed model to explain the failure mechanism for the three shapes: **(i)**: Hexagon; **(ii)**: Triangle; **(iii)**: Quadrilateral. **(a)** Experimental images taken at the supporting segment switching moment for each shape. **(b)** Diagrams illustrating the proposed model. The theoretical maximum pitch angle for the robot to produce sustained rolling, β_m, is computed as the largest slope angle which the robot with each shape can climb up. In (a) and (b), red circle represent robot CoM. Green and yellow highlighted segment represent the current and next supporting segments, respectively. $[x_l, x_u]$ represent the effective region of supporting polygon (ERSP). **(c)** Experimentally-measured robot step length, plotted against the robot's instantaneous body pitch angle at the supporting segment switching moment during each step. Black vertical line represents the model-predicted critical pitch angle, beyond which the robot would fail to achieve supporting segment switching and sustainable rolling. Pink shaded regions represent the model-predicted failure region.

for the Quadrilateral. To test our hypothesis about the failure mechanism, we compared the model-predicted maximum pitch angles with experimental measurements. Fig. 6c shows the experimentally-measured robot step lengths plotted against the instantaneous robot pitch angles at the supporting segment switching moment. If our hypothesis was correct, when the robot pitch is larger than β_m, the robot step length would either decrease to 0 or became negative (*i.e.,* falling backwards).

We found that the experimental measurements agreed well with the model-predicted critical pitch angle: most steps with pitch angle smaller than β_m (Fig. 6c, black vertical line) exhibited positive step length, whereas steps with pitch angle larger than β_m exhibited 0 or negative step length. We noted that there were two steps in Triangle shape where failures occurred at relatively small pitch (Fig. 6c-ii, lower left). We believed this is due to the feedback effect where the robot-substrate interaction during the previous failure steps disturbed local substrate profile such as slope or strength, causing a greater disturbances for future steps. This feedback effect was also observed and reported in several recent studies [12], [28], [29].

The model-predicted β_m for explained the experimentally-observed sand-rolling performance among different shapes. Based on the model prediction, the maximal pitch angle for Hexagon and Triangle to produce sustainable rolling was significantly smaller as compared to the Quadrilateral. As a result, the Hexagon and Triangle shapes exhibited higher failure rate on sand, whereas the Quadrilateral exhibited the most stable rolling. The understanding of the failure mechanism also provides valuable insights to inform design adaptations to improve sand-rolling performance for Hexagon and Triangle (Sec. IV).

IV. Model-informed design adaptation for improved sand-rolling performance

Based on the discovered failure mechanism, we proposed a simple design adaptations to improve robot's rolling performance on sand. Specifically, we attached L-shaped brackets connected with horizontal bars on the outside of the segments (Fig. 7b). We expected the added segments to improve the robot's sand-rolling performance through two mechanisms: (i) increasing the sand penetration resistance force [30], [31] on the supporting segment. The increased penetration resistance force could reduce the sinkage on the back end of the segment, and therefore reducing the associated body pitch to remain below β_m, preventing the observed oscillation-in-place failure (Fig. 6). (ii) increasing the sand shear resistive force [32], [33] on the supporting segment, to reduce the slippage of the supporting segment and increase the robot's displacement during the stance.

To test the effectiveness of the proposed design adaptation, we compared the experimentally-measured robot step lengths and pitch angles between with and without the adaptation for each shape. Results shown that the proposed adaptation could significantly reduce the failure rate for the two "high speed, high failure rate" shapes, Hexagon and Triangle, and allowed them to produce sustained rolling on sand. Fig. 7 shows the comparison of step length and pitch angle for the Triangle shape on sand. With the simple adaptation, the averaged pitch angle was reduced by 30%, improving the averaged step length by more than 200%. In addition, with the adaptation the failure rate was decreased from 66% to 0.

The significantly improved step length and success rate demonstrated that by better understanding the failure mechanism, the robot could utilize extremely simple adaptations to achieve fast and robust rolling on deformable sand.

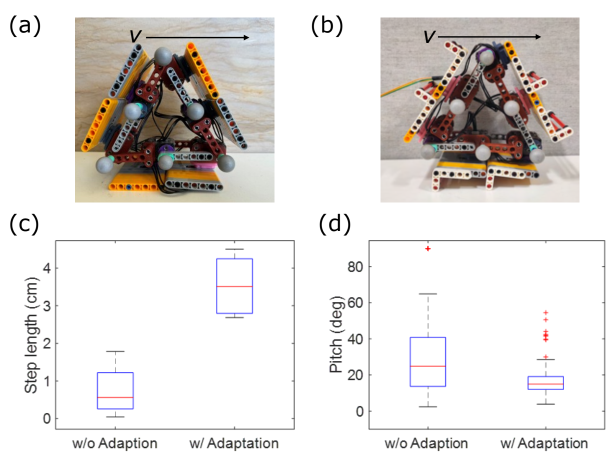

Fig. 7. The proposed design adaptation to improve robot's sand-rolling performance. **(a)** A side-view image of the robot without the adaptations.**(b)** A side-view image of the robot with the proposed adaptation. **(c)** Comparison of robot's step length on sand between the two different configurations. **(d)** Comparison of robot's max pitch angle in each step between the two different configurations.

V. Conclusion

In this study, we developed a novel sand-rolling robot that is capable of traversing both rigid and deformable surfaces with different body shapes. We investigated how the robot body shape affects the rolling performance on sand, and found that Quadrilateral shape produced the most stable rolling, whereas the Hexagon and Triangle shapes can generate effective rolling initially but exhibited frequent failure after a few steps. Through the analysis of robot dynamics and interaction with the deformable substrates, we discovered that the ability for the robot to produce sustainable rolling on sand was largely dependant on the pitch angle of the robot during supporting segment switching. We developed a simple model that allows prediction of the critical pitch angle for each shape to effectively achieve sustained rolling. The model prediction agreed well with experimental measurements, and informed a simple design adaptation that successfully reduced the pitch angle and failure rate for Triangle and Hexagon, and improved their rolling speeds on sand by more than two folds.

The insights gained from this study can guide novel design and locomotion control strategies for robots to traverse deformable substrates where traditional robots may struggle. By providing a better understanding of robot-sand interaction, our study takes a substantial step forward towards the development of robotic systems that can flexibly cope with complex, natural environments and assist with a wide variety of applications.

Acknowledgment

This research is supported by funding from the National Science Foundation (NSF) CAREER award #2240075, the NASA Planetary Science and Technology Through Analog Research (PSTAR) program, Award # 80NSSC22K1313, and the NASA Lunar Surface Technology Research (LuSTR) program, Award # 80NSSC24K0127. The authors would like to thank Liam Hall for helping with the robot design.

References

[1] H. M. Jaeger and S. R. Nagel, "Physics of the granular state," *Science*, vol. 255, no. 5051, pp. 1523–1531, 1992.

[2] M. G. Bekker, "Theory of land locomotion," 1956.

[3] J. Y. Wong *et al.*, *Terramechanics and off-road vehicles.* Elsevier, 1989.

[4] C. Sorice, K. S. Ali, A. Trebi-Ollennu, P. Mishra, G. Lim, P. Bailey, T. L. Hudson, E. Marteau, and J. Kim, "Insight robotic arm testing activities for hp3 mole anomaly recovery on mars," in *2021 IEEE Aerospace Conference (50100).* IEEE, 2021, pp. 1–19.

[5] R. D. Maladen, Y. Ding, C. Li, and D. I. Goldman, "Undulatory swimming in sand: subsurface locomotion of the sandfish lizard," *science*, vol. 325, no. 5938, pp. 314–318, 2009.

[6] N. Mazouchova, P. B. Umbanhowar, and D. I. Goldman, "Flipper-driven terrestrial locomotion of a sea turtle-inspired robot," *Bioinspiration & biomimetics*, vol. 8, no. 2, p. 026007, 2013.

[7] H. Marvi, C. Gong, N. Gravish, H. Astley, M. Travers, R. L. Hatton, J. R. Mendelson, H. Choset, D. L. Hu, and D. I. Goldman, "Sidewinding with minimal slip: Snake and robot ascent of sandy slopes," *Science*, vol. 346, no. 6206, pp. 224–229, 2014.

[8] F. Qian, T. Zhang, W. Korff, P. B. Umbanhowar, R. J. Full, and D. I. Goldman, "Principles of appendage design in robots and animals determining terradynamic performance on flowable ground," *Bioinspiration & biomimetics*, vol. 10, no. 5, p. 056014, 2015.

[9] B. McInroe, H. C. Astley, C. Gong, S. M. Kawano, P. E. Schiebel, J. M. Rieser, H. Choset, R. W. Blob, and D. I. Goldman, "Tail use improves performance on soft substrates in models of early vertebrate land locomotors," *Science*, vol. 353, no. 6295, pp. 154–158, 2016.

[10] H. C. Astley, J. R. Mendelson III, J. Dai, C. Gong, B. Chong, J. M. Rieser, P. E. Schiebel, S. S. Sharpe, R. L. Hatton, H. Choset *et al.*, "Surprising simplicities and syntheses in limbless self-propulsion in sand," *Journal of Experimental Biology*, vol. 223, no. 5, p. jeb103564, 2020.

[11] R. D. Maladen, Y. Ding, P. B. Umbanhowar, and D. I. Goldman, "Undulatory swimming in sand: experimental and simulation studies of a robotic sandfish," *The International Journal of Robotics Research*, vol. 30, no. 7, pp. 793–805, 2011.

[12] C. Li, P. B. Umbanhowar, H. Komsuoglu, D. E. Koditschek, and D. I. Goldman, "Sensitive dependence of the motion of a legged robot on granular media," *Proceedings of the National Academy of Sciences*, vol. 106, no. 9, pp. 3029–3034, 2009.

[13] F. Qian, T. Zhang, C. Li, P. Masarati, A. M. Hoover, P. Birkmeyer, A. Pullin, R. S. Fearing, and D. I. Goldman, "Walking and running on yielding and fluidizing ground," *Robotics: Science and Systems*, p. 345, 2013.

[14] X. A. Wu, T. M. Huh, A. Sabin, S. A. Suresh, and M. R. Cutkosky, "Tactile sensing and terrain-based gait control for small legged robots," *IEEE Transactions on Robotics*, vol. 36, no. 1, pp. 15–27, 2019.

[15] W. W. A. J. Z. D. W. Haomachai, D. Shao and P. Manoonpong, "Lateral undulation of the bendable body of a gecko-inspired robot for energy-efficient inclined surface climbing," *IEEE robotics and automation letters*, vol. 6, no. 4, pp. 7917–7924, 2021.

[16] R. K. O. Guetta, D. Shachaf and D. Zarrouk, "A novel wave-like crawling robot has excellent swimming capabilities," *Bioinspiration biomimetics*, vol. 18, no. 2, pp. 26 006–, 2023.

[17] J. Downer, "Weird nature: an astonishing exploration of nature's strangest behavior, 2002."

[18] K. H. B. N. A. Najbar, A. Konowalik and M. Ogielska, "Body size and life history traits of the fire salamander salamandra salamandra from poland," *Amphibia-reptilia*, vol. 41, no. 1, pp. 63–74, 2020.

[19] H. B. B. S. B. R. N. A. Mansour, T. Jang and Y. Kim, "Compliant closed-chain rolling robot using modular unidirectional sma actuators," *Sensors and actuators. A. Physical.*, vol. 310, pp. 112 024–, 2020.

[20] E. Steltz, A. Mozeika, N. Rodenberg, E. Brown, and H. Jaeger, "Jsel: Jamming skin enabled locomotion," *2009 IEEE/RSJ International Conference on Intelligent Robots and Systems*, vol. 0, no. 0, pp. 5672–5677, 2009.

[21] J. Aguilar and D. I. Goldman, "Robophysical study of jumping dynamics on granular media," *Nature Physics*, vol. 12, no. 3, pp. 278–283, 2016.

[22] C. Li, T. Zhang, and D. I. Goldman, "A terradynamics of legged locomotion on granular media," *science*, vol. 339, no. 6126, pp. 1408–1412, 2013.

[23] W. W. Dickinson and J. D. Ward, "Low depositional porosity in eolian sands and sandstones, namib desert," *Journal of Sedimentary Research*, vol. 64, no. 2a, pp. 226–232, 1994.

[24] R. B. McGhee and A. A. Frank, "On the stability properties of quadruped creeping gaits," *Mathematical Biosciences*, vol. 3, pp. 331–351, 1968.

[25] M. Kalakrishnan, J. Buchli, P. Pastor, M. Mistry, and S. Schaal, "Fast, robust quadruped locomotion over challenging terrain," in *2010 IEEE International Conference on Robotics and Automation*. IEEE, 2010, pp. 2665–2670.

[26] W. Li, W. Zhang, Q. Gao, Q. Guo, S. Wu, H. Zou, Z. Peng, and G. Meng, "Electrically activated soft robots: Speed up by rolling," *Soft Robotics*, vol. 8, no. 5, pp. 611–624, 2021.

[27] R. M. Nedderman *et al.*, *Statics and kinematics of granular materials*. Cambridge University Press Cambridge, 1992, vol. 352.

[28] S. Liu, B. Huang, and F. Qian, "Adaptation of flipper-mud interactions enables effective terrestrial locomotion on muddy substrates," *IEEE Robotics and Automation Letters*, 2023.

[29] S. Shrivastava, A. Karsai, Y. O. Aydin, R. Pettinger, W. Bluethmann, R. O. Ambrose, and D. I. Goldman, "Material remodeling and unconventional gaits facilitate locomotion of a robophysical rover over granular terrain," *Science robotics*, vol. 5, no. 42, p. eaba3499, 2020.

[30] G. Hill, S. Yeung, and S. A. Koehler, "Scaling vertical drag forces in granular media," *Europhysics Letters*, vol. 72, no. 1, p. 137, 2005.

[31] T. A. Brzinski III, P. Mayor, and D. J. Durian, "Depth-dependent resistance of granular media to vertical penetration," *Physical review letters*, vol. 111, no. 16, p. 168002, 2013.

[32] R. Albert, M. Pfeifer, A.-L. Barabási, and P. Schiffer, "Slow drag in a granular medium," *Physical review letters*, vol. 82, no. 1, p. 205, 1999.

[33] I. Albert, P. Tegzes, R. Albert, J. Sample, A.-L. Barabási, T. Vicsek, B. Kahng, and P. Schiffer, "Stick-slip fluctuations in granular drag," *Physical Review E*, vol. 64, no. 3, p. 031307, 2001.